Springer

Available online at https://link.springer.com/journal/42241
http://www.jhydrodynamics.com
Journal of Hydrodynamics, XXX, XXX(XXX): XXX–XXX
https://doi.org/10.1007/s42241-XXX-XXXX-X

On wave breaking and instabilities

F. Dias[1,2,4*], M. R. Turner[3], A. Mansar[1], T. J. Bridges[3]

1. Centre Borelli, ENS Paris-Saclay, Gif-sur-Yvette, France
2. School of Mathematics and Statistics, University College Dublin, Dublin, Ireland
3. School of Mathematics and Physics, University of Surrey, Guildford, UK
4. Institut Universitaire de France, Paris, France

(Received month, date, year, Revised month, date, year, Accepted month, date, year, Published online month, date, year)
© China Ship Scientific Research Center 2026

Abstract: The instability of water waves is a topic with a long history. After reviewing some of the key developments in the study of water wave instabilities, we revisit an interesting link between the so-called superharmonic instability and wave breaking.

Key words: water waves, instabilities, horse-shoe patterns, dipole, Stokes waves, eigenfunctions, wave breaking

0. Introduction

When evaluating the stability of nonlinear periodic water waves, like Stokes wave, perturbations can be classified by perturbation periodicity or by resonance geometry. In the former case, perturbations are categorized by how their spatial period compares to the carrier wave's period. When the spatial period is larger than the carrier wave, the instability is subharmonic. The modulational instability is a special case where the perturbation represents a long-wavelength modulation of the wave envelope. When the spatial period is the same or smaller than the carrier wave, the instability is superharmonic. In the latter case, perturbations are categorized by the order of the resonant interactions between the carrier wave and small sideband perturbations. Instabilities are then split into Class I and Class II based on the dominant $N-$wave resonance mechanism ($N = 4$ for Class I instabilities, $N = 5$ for Class II instabilities).

One of the most fascinating discoveries in the field of water waves is the discovery of the modulational instability as a consequence of a laboratory experiment that went wrong. The modulational instability is best described as follows: Take as an initial condition a monochromatic deep-water wave (a Stokes wave) with a small disturbance added in the form of modulation with a wavelength much larger than the wavelength of the carrier. It turns out that for some values of the steepness the wave is linearly unstable with respect to this long-wave perturbation. The history of the discovery goes as follows[1]. In 1963 Benjamin's student Jim Feir was measuring the waves along a new 10-m tank in Cambridge, UK. Waves started as a regular train with constant frequency and wavelength, but then about 5 m down the tank began to form into groups. The first guess was that it was due to imperfections in the construction and operation of the wave maker. Feir moved to the much larger wave tank in the National Physical Laboratory. Several modulating frequencies and amplitudes were imposed on the wave maker. The observations were similar! Benjamin and Feir[2] performed a linear analysis of a deep-water Stokes wave perturbed by two sidebands, leading to predictions of sideband growth rate as the wave slope increased. Benjamin[3] extended the analysis to waves on water of arbitrary depth. The process of nonlinear focusing ceases to exist when $kd < 1.363$, where k is the wave number and d the water depth. Note that both papers[2] and[3] refer to a third paper to appear in the Journal of Fluid Mechanics as Part 2 (Experiments) but as far as we know this experimental paper was never published. Interestingly the modulational instability was discovered in optics at about the same time, although independently[4]. Numerical simulations such as those shown in Fig. 1 - see for example[5] - clearly illustrate the modulational instability. Starting from an almost sinusoidal train of waves, one sees that one wave pumps energy from its neighbors to become larger. But this phenomenon is recurrent: indeed the neighbors suck the energy from the larger wave and the train of waves gradually reaches its original shape, and then a new cycle starts. This recurrence of the modulational instability was well understood by Fermi, Pasta, Ulam and Tsingou. Inter-

Project supported by the ERC (Grant No. 833125).
Corresponding author: Frédéric Dias,
E-mail: frederic.dias@ens-paris-saclay.fr

estingly, the first numerical simulations of this recurrence were performed by Tsingou but her name only appeared in a remark in the report that was written by Fermi, Pasta and Ulam[6].

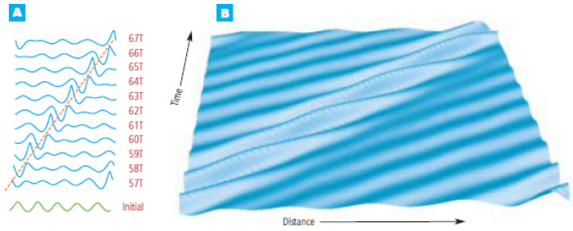


Fig. 1 Illustration of the modulational instability: surface elevation in a time-space representation (during 10 wave periods)

In the late 1970s and early 1980s, several papers dealing with instabilities of water waves were published. In 1978, Longuet–Higgins coined the terminology "superharmonic instability"[7]. The distinguishing feature of that instability is that the perturbations have the same horizontal scale as the fundamental wave, or less. Longuet–Higgins focuses on perturbations with the same basic wavelength. This feature is to be contrasted with subharmonic instabilities and the modulational (Benjamin-Feir) instability where the perturbation has a longer wavelength – see above. In fact, Longuet–Higgins wrote a companion paper[8] devoted to subharmonics instabilities. Interestingly, Longuet–Higgins writes that "the calculations of the subharmonics can be carried out by a relatively simple modification of the analysis" of the "superharmonics" paper. In 1982, McLean explicitly introduced and categorized Class I and Class II instabilities while studying the three-dimensional stability of finite-amplitude Stokes waves[9]. Class I instabilities correspond to quartet resonant interactions (the modulational instability falls under this class) while Class II instabilities correspond to quintet resonant interactions (these instabilities can lead to the formation of distinct crescent-shaped or horseshoe wave patterns). McLean demonstrated that while Class I instabilities typically dominate at lower wave steepness values, Class II instabilities take over and dominate as the waves become steep, ultimately driving three-dimensional wave breaking.

In fact the link between wave breaking and instabilities has been made several times. For example one can find in Babanin's book on the breaking and dissipation of ocean surface waves[10] the following statement: "Instability is a key word in the breaking process". However Babanin also writes that "Some processes leading to wave breaking, and in particular the most important mechanism of modulational instability of nonlinear wave trains, may be impaired in three-dimensional natural field circumstances, which fact further depletes the generality of conclusions achieved in two-dimensional wave tanks". But which instabilities are the most relevant for wave breaking?

The superharmonic instability develops into a crest instability. For the case of unstable periodic Stokes waves, the wave-breaking scenario was observed in the numerical simulations of Jillians[11] and of Longuet–Higgins and Dommermuth[12]. Jillians took the accurately resolved eigenfunction as a small perturbation to the Stokes wave and integrated in time. Note that there are two eigenmodes: a growing one and a decaying one. In this review, we focus on the growing eigenmode of the superharmonic instability. A microbreaker emerged from the superposition of a periodic travelling wave and a superharmonic unstable eigenfunction. Fig. 2 clearly shows the dipole shape obtained by taking the difference between the wave and the steady Stokes wave profile.

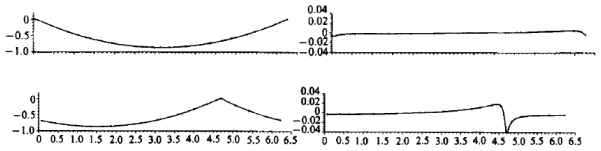


Fig. 2 Illustration of the crest instability. The profiles on the left are those of the wave and the profiles on the right are those of the disturbance. The first row is at the initial time (Stokes wave on the left and eigenmode on the right). The second row is at a later time. Adapted from[11]

Mansar et al.[13] checked the robustness of the appearance of this crest instability leading to breaking. They added a perturbation to a large-amplitude unstable Stokes wave, which was then taken as initial data in a direct numerical solution of the Navier-Stokes equations, using the Basilisk numerical software package. Mansar et al.[13] used the Singular Value Decomposition (SVD) to extract and isolate the unstable wave modes growing on a background 2D Stokes wave. Their SVD analysis successfully captured a distinct dipole shape concentrated around the wave crest, confirming the underlying geometric mechanism that drives localized overtopping and wave breaking.

The paper is organized as follows. In the first section, we revisit Class I and Class II instabilities and try to find out where the superharmonic instability fits in. In the second section, we focus on crest instabilities. We review the instability of 2D Stokes waves travelling in deep water. We find that these waves are susceptible to a crest instability at large amplitude, with a dipole structure of the eigenfunctions that varies periodically along the crest. Studying the full 2D problem numerically, with the unstable eigenfunctions as initial data, leads to overturning crests that generate the structure of a microbreaker, similar to what has been observed in

the open ocean.

1. Revisit of Class I and Class II instabilities

McLean[9] performed a numerical investigation of normal-mode perturbations of a finite-amplitude Stokes wave travelling at speed c in deep water. In the frame of reference moving with the speed c, the base flow is computed as

$$\overline{\eta}(\widehat{x}) = \sum_{n=0}^{\infty} A_n \cos(nk_0\widehat{x}), \tag{1}$$

$$\overline{\Phi}(\widehat{x},\widehat{z}) = -c\widehat{x} + \sum_{n=1}^{\infty} B_n \sin(nk_0\widehat{x})e^{n\widehat{z}}, \tag{2}$$

where $\overline{\eta}$ is the free-surface elevation, $\overline{\Phi}$ is the velocity potential, $\widehat{x}$ and $\widehat{z}$ are respectively the horizontal and vertical coordinates, and k_0 is the wavenumber of the 2D Stokes wave. The mean water level is given by $\widehat{z} = 0$. The idea is as follows. One introduces perturbations to the base flow in the frame of reference moving with the wave, writing

$$\eta(\widehat{x},\widehat{y},t) = \overline{\eta}(\widehat{x}) + \eta'(\widehat{x},\widehat{y},t), \tag{3}$$

$$\Phi(\widehat{x},\widehat{y},\widehat{z},t) = \overline{\Phi}(\widehat{x},\widehat{z}) + \Phi'(\widehat{x},\widehat{y},\widehat{z},t), \tag{4}$$

where an overbar signifies a base flow component, and the primes signify perturbation fields, which are small with $|\eta'| \ll |\overline{\eta}|$ and $|\Phi'| \ll |\overline{\Phi}|$. The transverse coordinate is denoted by $\widehat{y}$. The perturbation fields are expanded in a double Fourier series, harmonically related to the basic state,

$$\eta' = e^{-\mathrm{i}\sigma t}e^{\mathrm{i}(p\widehat{x}+q\widehat{y})}\sum_{j=-\infty}^{\infty} a_j e^{\mathrm{i}j\widehat{x}}, \tag{5}$$

$$\Phi' = e^{-\mathrm{i}\sigma t}e^{\mathrm{i}(p\widehat{x}+q\widehat{y})}\sum_{j=-\infty}^{\infty} b_j e^{\mathrm{i}j\widehat{x}}e^{\alpha_j\widehat{z}}, \tag{6}$$

where $\sigma \in \mathbb{C}$ is the stability exponent, with $\mathrm{Im}(\sigma) > 0$ signifying instability and $\alpha_j^2 = (p+j)^2 + q^2$. The parameters p and q are the dimensionless wavenumbers of the perturbation, relative to the underlying Stokes wave, and the form of α_j in the exponent is required, such that Φ' is a solution to Laplace's equation. McLean found that, for small amplitude waves, the dominant instability is two-dimensional (of Benjamin–Feir type) but, for larger amplitudes, the dominant instability becomes a three-dimensional perturbation ($q \neq 0$). It is common to read in the literature that the mechanism responsible for Class I instabilities is a four-wave resonance while the mechanism responsible for the Class II instability is a five-wave resonance. But one has to be cautious because in some cases the same wave is repeated twice or three times when counting the four waves or the five waves. Melville[14] performed experiments on the instability and breaking of 2D deep-water waves. However, he noticed that the 2D waves could be subject to 3D instabilities as seen in Fig. 3. This is described in an appendix of his paper.

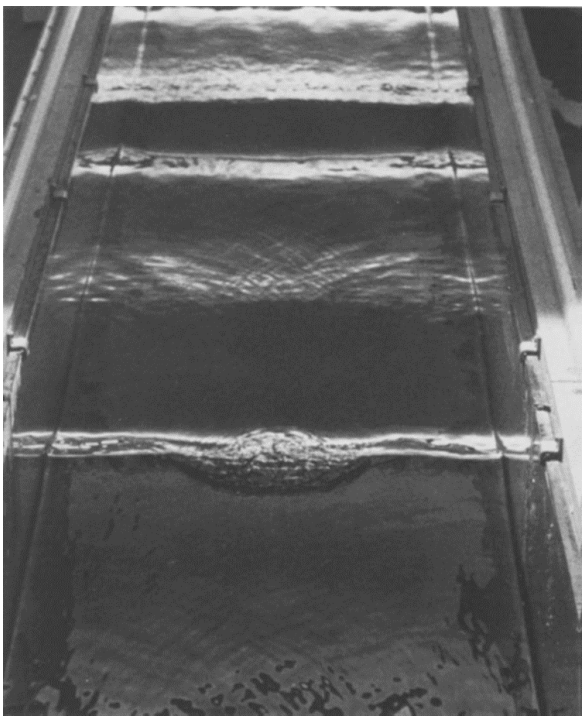


Fig. 3 3D instability of 2D waves in a channel[14]

McLean[9] provided plots of the instability regions for several values of the steepness defined as the ratio between the crest-to-trough height h and the wavelength λ: $h/\lambda = 0.032$, 0.064, 0.095, 0.111, 0.127 and 0.131. He also provided a plot of the curves for four- and five-wave resonances from the linear dispersion relation. When the steepness is low, the class I instability dominates. As the steepness increases, the class II instability becomes more and more important and the class I instability eventually disappears. The instability plots can be referred to as the (p,q) plots, where pk_0 is the wavenumber of the perturbation in the direction of the wave and qk_0 is the wavenumber of the perturbation in the transverse direction. Above a certain threshold for the wave steepness, the region of the class II instability hits the $p-$axis at the value $p = 1/2$. Moreover at $p = 1/2$, the instability is co-propagating with the unperturbed wave (the real part $\mathrm{Re}(\sigma)$ in $\exp(-\mathrm{i}\sigma t)$ is zero). This implies that steady 3D waves bifurcate from 2D waves at the point of stability exchange with $p = 1/2$. Meiron et al.[15] computed such 3D waves. These 3D waves have symmetric fronts as shown in Fig. 4.

Experiments were also performed to check the

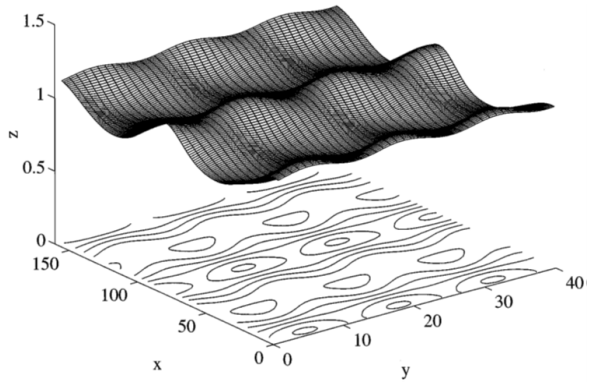


Fig. 4 Steady 3D waves bifurcating from 2D waves[15]

physical existence of these 3D waves both in a long tow tank and in a wide basin. Su et al.[16] observed 3D structures corresponding to the nonlinear evolution of the dominant instability discovered by McLean[9]. The initial 2D wave train of large steepness evolves into a series of 3D spilling breakers, followed by a transition to a more or less 2D wave train. These 3D patterns take the form of crescent-shaped perturbations (horse-shoe patterns) riding on the basic waves as shown in Fig. 5. Su[17] observed the formation of the bifurcated 3D symmetric waves. A theory for these horse-shoe patterns is proposed in Shrira et al.[18].



Fig. 5 Horse-shoe patterns[17]

Roughly speaking, the study of McLean was limited to small or medium amplitudes. Kharif[19] extended it to larger amplitudes, from a steepness of 0.131 to a steepness of 0.137. At a steepness of 0.131, McLean found that the dominant instability is a Class II instability with $p = 1/2$ and $q = 0.65$, together with the real part of σ equal to 0. At a steepness of 0.137, Kharif found that the dominant instability is a Class II instability with $p = 1/2$ and $q = 0$, together with the real part of σ equal to 0. The dominant class II instability is thus no longer predominantly 3D. Kharif noticed that the steepness of 0.137 also corresponds to the first maximum of wave energy as a function of wave steepness. But neither McLean nor Kharif provided plots of the eigenfunctions. This is why we decided to redo these stability computations.

1.1 *Validity check*

Algorithms in the literature are used as a starting point for our analysis. However, the Stokes waves and their linear stability are computed from scratch using a Fourier spectral method. This subsection shows the McLean's plots reproduced by ourselves and based on equations (1)-(2) and (5)-(6). We start with a low steepness as shown in Fig. 6. The 0.111 steepness case is the same as figure 2(d) of McLean showing the class I and class II instability regions. The square and circle denote their respective maximum growth rates, and the red shading is darker at larger values of $\mathrm{Im}(\sigma)$ and lighter at smaller values. The 0.131 steepness case,

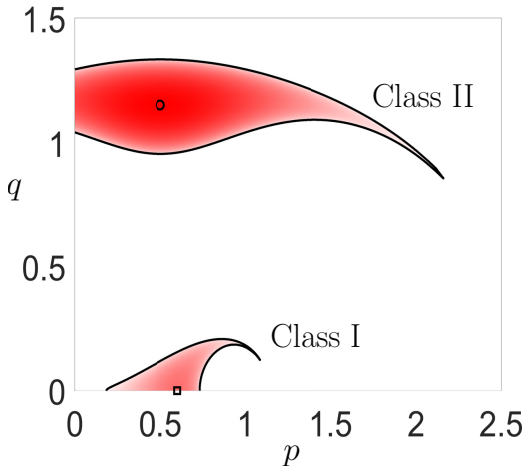


Fig. 6 Stability plot. The steepness is 0.111. The red color indicates instability.

shown in Fig. 7, is the same as figure 2(f) of McLean showing that the class I region vanishes as the steepness increases.

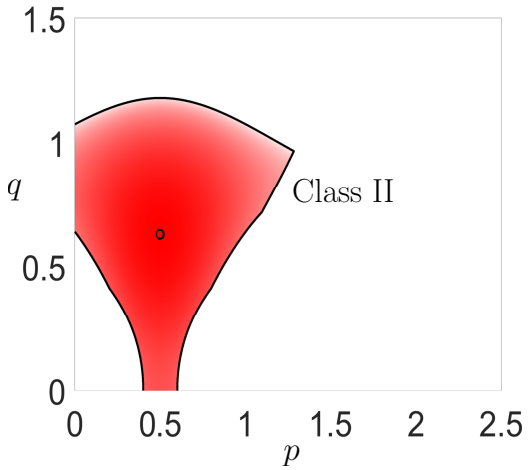


Fig. 7 Stability plot. The steepness is 0.131.

Next, like Kharif, we increase the steepness beyond the highest value considered by McLean (see

Kharif[19], [20] for a comparison of the relative strength of class I versus class II instabilities and[21]). Here we consider stability regions of the Class II modes, while Kharif's plots focus on the stability region of the Class I modes. Kharif[19] shows that the stability region of the Class I modes becomes increasingly small as the steepness increases, while here we find the Class II instability region remains finite in size as the steepness increases.

The 0.136 steepness case shown in Fig. 8 shows that the region reduces in size, and the value of $q = 0.27$ at the maximum growth rate moves towards $q = 0$. The maximum growth rate in fact reaches $q = 0$ at

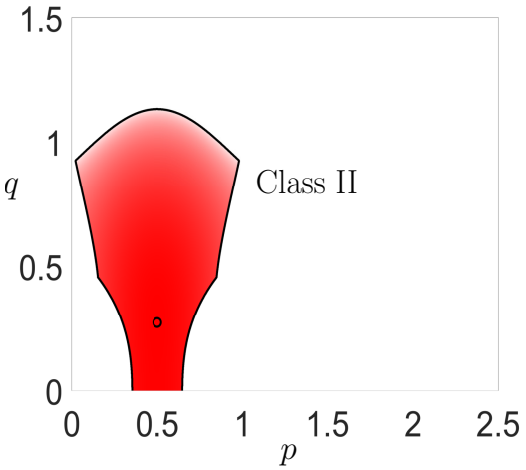


Fig. 8 Stability plot. The steepness is 0.136.

a steepness equal to 0.13661 (note that this value was rounded to 0.137 above). This value, when multiplied by π, is equivalent to the 0.4292 value found in Mansar et al.[13]. The value is also mentioned by Tanaka[22] for the change of stability of a 2D Stokes wave. The difference with the McLean paper is a rescaling of the wavelength of the waves by π. Longuet–Higgins suggested in his paper that the stability change of the 2D Stokes wave might occur at the steepest wave value (because his numerics were not accurate enough to get closer to that point), and then Tanaka showed it was actually at a smaller steepness value. McLean hinted that the class II modes would have $q = 0$ at the steepest wave value, but we have shown that actually it occurs earlier, and at this value 0.13661, which is significant to the 2D Stokes wave. The value 0.13661 for the steepness (or 0.4292 if multiplied by π) is quite significant. At this value, the wave energy is maximum, the dominant class II instability becomes 2D and the superharmonic instability kicks in. The stability plot is shown in Fig. 9. Given the fact that Kharif's paper is almost 40 years old, we were able to increase the steepness even further. The value of q stays zero for a small range of wave steepnesses and then becomes non-zero again as the steepest wave is approached. As this happens the maximum growth

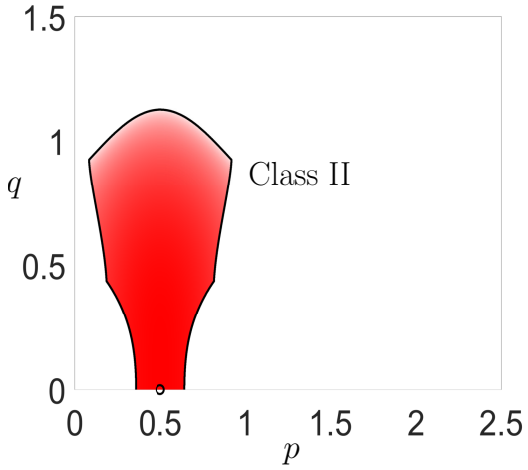


Fig. 9 Stability plot. The steepness is 0.13661. The maximum growth rate occurs at $q = 0$.

rate of the class II modes keeps increasing. The 0.1385 steepness case shown in Fig. 10 is new and shows the stability region continues to shrink, and the value of $q = 0.35$ of this maximum is again non-zero.

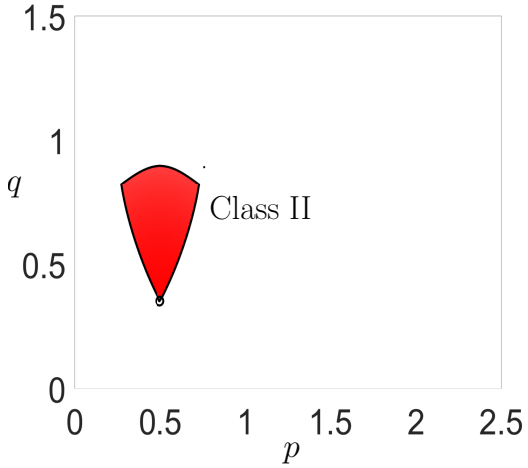


Fig. 10 Stability plot. The steepness is 0.1385.

The other two figures Fig. 11 and Fig. 12 give the maximum values of the growth rate $\mathrm{Im}(\sigma)$, and the corresponding p and q values as a function of the steepness h/λ. Note, the class I modes always have $q = 0$, and p varies, whereas the class II modes always have $p = 0.5$ and q varies. The solid lines are the class II modes and the dashed line is the class I mode. In both figures the vertical dotted line is the steepest wave $h/\lambda = 0.141$, and in the (p, q) plane the vertical dot-dash line is the value $h/\lambda = 0.13661$, which is the steepness value that the 2D Stokes wave ($p = q = 0$) goes unstable. The square and circles in the (p, q) plane and growth rate plot correspond to the values in the stability region figures.

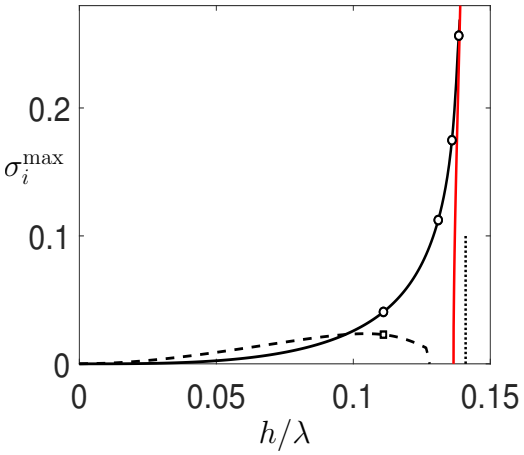


Fig. 11 Maximum values of the growth rate Im(σ). The Class I mode growth rate is given by the dashed curve, while the Class II mode growth rate is given by the solid curve. The red curve represents the growth rate of the $p = q = 0$ superharmonic instability. This mode has a growth rate which increases very rapidly and eventually becomes the dominant mode over the 2D class II mode.

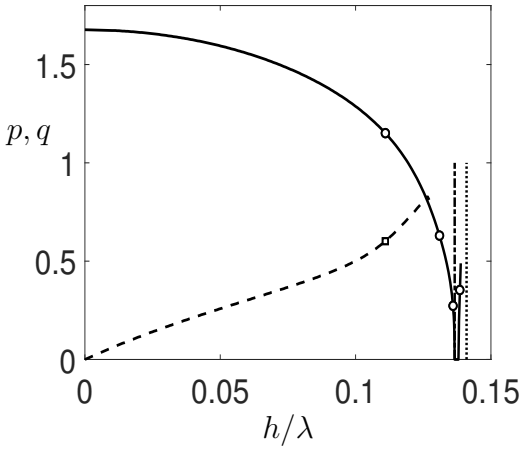


Fig. 12 Corresponding p (dashed curve) and q (solid curve) values to those in figure 11.

2. Wave breaking

Experiments and observations on breaking waves pick up in the 1990s with a key reference being the review paper of Banner and Peregrine[23]. In their paper, they also synthesize decades of research mapping out how surface gravity waves grow unstable and transition to breaking. Both Class I and Class II instabilities can lead to wave breaking. While most papers on wave breaking and instabilities mention the growth rate of the instability, very few look at the eigenmodes associated with the instability. When a periodic wave grows large enough to enter the superharmonic unstable regime, its unstable eigenfunction develops a distinct dipole-like shape concentrated tightly around the wave crest. Longuet–Higgins and Dommermuth[12] showed that adding this dipole-shaped instability mode to the basic wave state, with the correct sign, dynamically increases the surface amplitude at the front of the crest, while lowering it immediately behind the crest. This asymmetrical deformation creates a physical mechanism for overtopping, where the water crest spills forward over the front face of the wave, initiating the breaking process. In this section we focus on the shape of the eigenmodes. We concentrate on 2D waves. We consider three kinds of instabilities: Class I, Class II and superharmonic instabilities.

2.1 *Breaking of 2D waves*

The breaking of 2D waves from the point of view of superharmonic instabilities was considered by Mansar et al.[13]. Therefore we refer to that paper for a full analysis. We only show results for comparison purposes. The unstable superharmonic modes were computed from scratch. First the basic state (2D periodic Stokes wave in infinite depth) is computed. The linear stability problem is derived by adding a perturbation to the basic state and linearising. The approach is similar to the approach of McLean[9], except that p and q are taken to be equal to 0 since all superharmonic instabilities have the same wavelength as the basic state. The eigenvalues and the eigenvectors are computed. The change in shape of the eigenfunction as σ goes from stable to unstable is shown in Fig. 13. The superharmonic instability kicks in when the steepness is equal to 0.13661, which is between the third and the fourth curves from the bottom, and at this point there is a topological change in the form of the eigenfunction, changing from sinusoidal to a dipolar form. This value is identified by fixing $p = q = 0$ and increasing the steepness until σ changes from real to purely imaginary.

While we were reviewing the Class II instability of 2D periodic waves, we saw that a critical value for steepness is 0.13661. Indeed the Class II instability becomes 2D. So what does the eigenmode looks like? It is shown in Fig. 14. The eigenmode has a double dipole shape. Since $p = 0.5$, it corresponds to a wavelength doubling instability, and so wave crests alternate being increased and decreased by the instability.

Next we look at the shape of the eigenmode for the Class I instability of 2D waves (modulational instability). See Fig. 15 for a periodic case ($p = 0.5$) and Fig. 16 for a non periodic case ($p = 0.6$). We don't see any indication of wave breaking as the dipole structure is less well pronounced. Finally, for the sake of completeness, we also show a 2D eigenmode in the case of a 3D Class II instability with $p = 0.5$ and $q = 1.15$. This is the 2D most unstable Class II mode for this particular steepness, see Fig. 17.

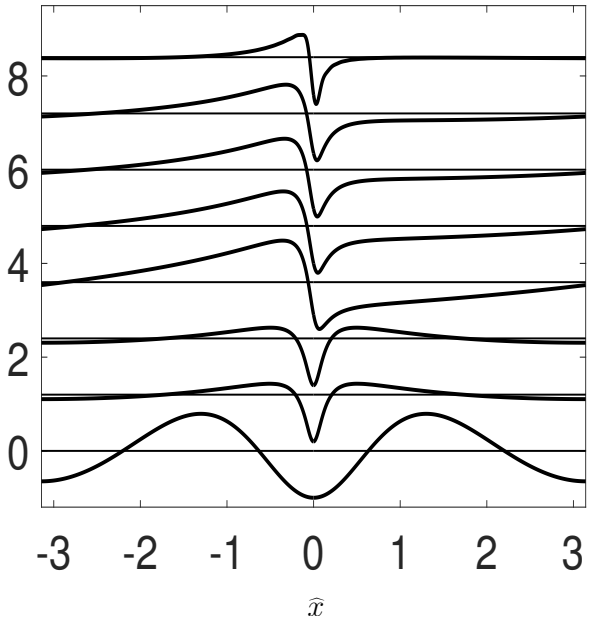


Fig. 13 Shape of the eigenmode (superharmonic instability) $\eta'(\widehat{x})$ plotted at wave steepness $h/\lambda = 0.064, 0.13640, 0.13655, 0.13671, 0.13687, 0.13703, 0.13719$ and 0.13932. Each eigenfunction is normalised so that its maximum is equal to 1, and the results are separated by a constant for clarity.[13]

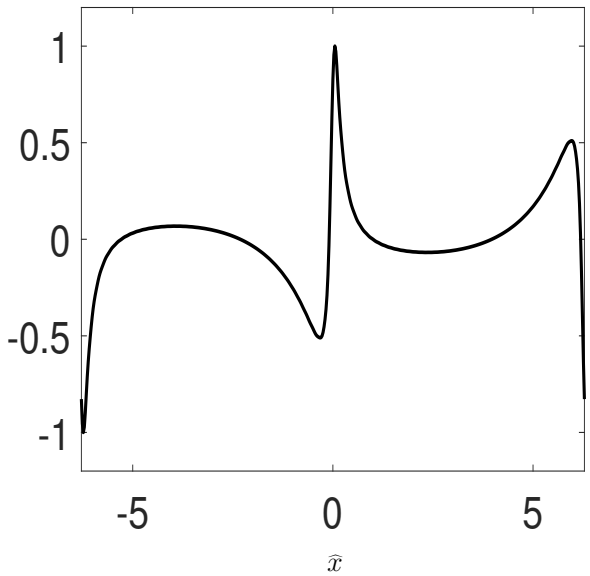


Fig. 14 Shape of the eigenmode (2D Class II instability with $p = 0.5$, $q = 0$) $\eta'(\widehat{x})$ plotted at wave steepness $h/\lambda = 0.13661$.

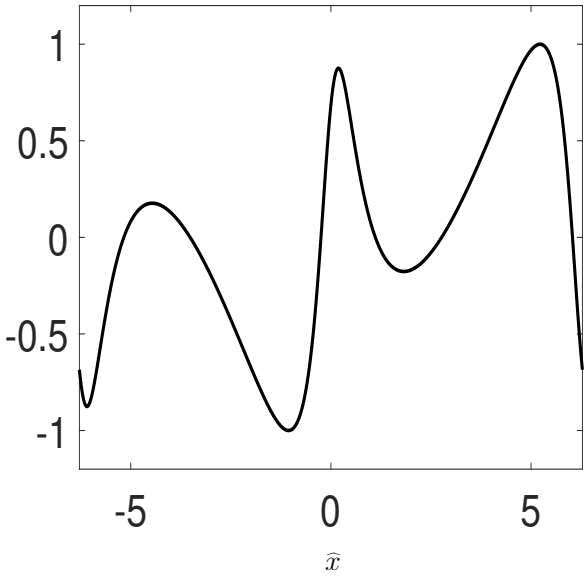


Fig. 15 Shape of the eigenmode (2D Class I instability with $p = 0.5$, $q = 0$) $\eta'(\widehat{x})$ plotted at wave steepness $h/\lambda = 0.111$.

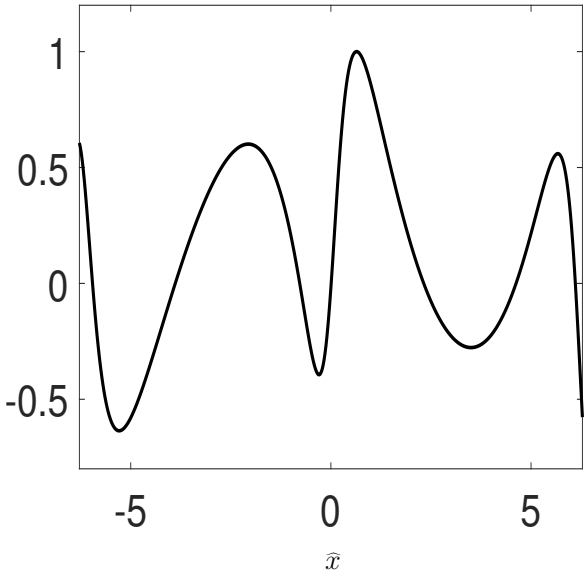


Fig. 16 Shape of the eigenmode (2D Class I instability with $p = 0.6$, $q = 0$) $\eta'(\widehat{x})$ plotted at wave steepness $h/\lambda = 0.111$. This is the maximum growth rate for this particular steepness.

2.2 *Numerical simulations*

Everything above is theoretical. In[13], in the context of the superharmonic instability, we tested the emergence of wave breaking to the presence of real-world perturbations. For the direct numerical simulation, we used the Basilisk software package[24-26].

The direct numerical simulations were initiated with data that approximate an unstable periodic Stokes wave. The incompressible two-phase formulation is used, with air above water. Previous studies have shown that inserting potential-flow solutions in a Navier-Stokes solver provides a suitable description of key breaking phenomena, including jet overturning, splash-up, gas entertainment, vorticity, and energy dissipation[27-32].

A fifth-order asymptotic Stokes wave solution by Fenton[33] is used to initialize the surface profile and velocity potential for inviscid, irrotational, periodic waves propagating over a fluid layer of finite depth. The period is T_0. The choice of the 5th-order solution for our two-phase simulations, instead of the fully numerical solution computed herein, was motivated by

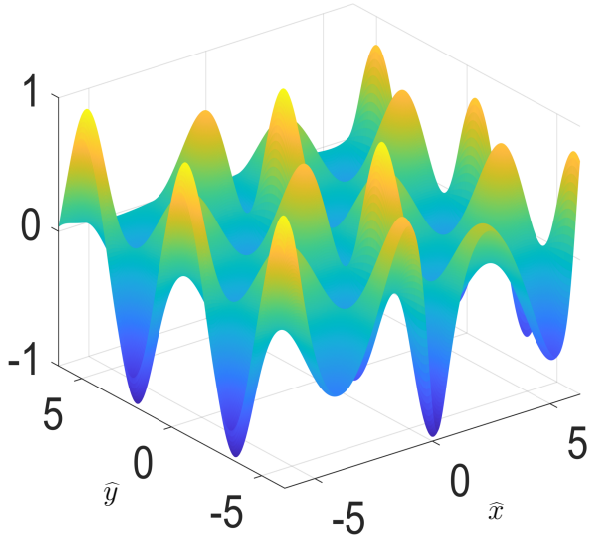


Fig. 17 Shape of the eigenmode (3D Class II instability with $p = 0.5$, $q = 1.15$) $\eta'(\widehat{x})$ plotted at wave steepness $h/\lambda = 0.111$.

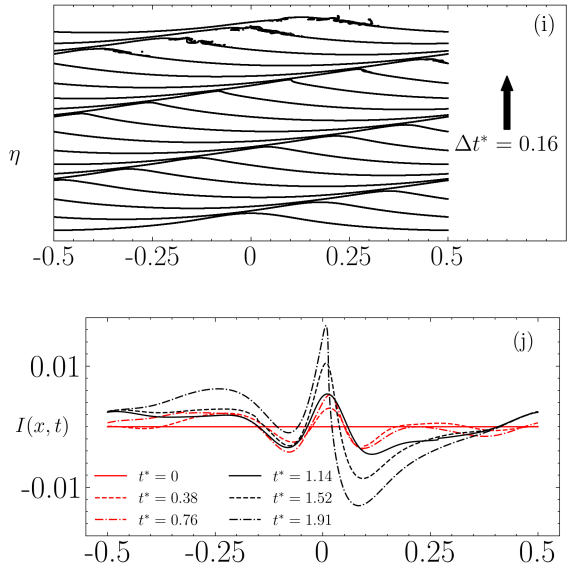


Fig. 18 Top: Evolution of the wave profile; Bottom: corresponding computed instability $I(x,t)$, where $t^* = t/T_0$ with T_0 the wave period. The wave steepness is $h/\lambda = 0.1241$.

balancing the proximity to real-world events offered by low-order analytical theories with the inclusion of higher-order harmonics provided by the 5th-order solution, which, as will be shown, are necessary for producing sufficiently steep nonbreaking waves.

The wave propagates horizontally in a square domain of length $L = \lambda$, with periodic boundary conditions in the direction of propagation and free-slip conditions at the top and bottom walls. An example of a breaking event corresponding to a simulation case with $h/\lambda = 0.1241$ is shown in Fig. 18 (top).

We quantify the evolution of instabilities by defining the variable $I(x,t)$,

$$I(x,t) = \eta_{\text{stat}}(x,t) - \eta(x,0), \tag{7}$$

where $\eta_{\text{stat}}(x,t) = \eta(x - U(t)t, t)$ is an approximation to the stationary wave, and represents the wave profile translated by the instantaneous crest velocity $U(t)$. This velocity is determined by fitting a third-order polynomial to the crest's location over time and then differentiating it to obtain the instantaneous crest velocity. An example of the outcome of this method to estimate the time evolution of the instability up to breaking is shown in Fig. 18 (bottom).

SVD was used to split the instability signal into distinct modes, each capturing a specific amount of energy. It is widely used for dimensionality reduction in applications such as image compression and forecasting[34].

Here, SVD is applied to the snapshot matrix $\boldsymbol{I}$, constructed from the vertical coordinates of the instability signal at spatial points uniformly distributed along the horizontal domain. The data are considered up to $t_f = 3T_0$ if no breaking occurs, or $t_f = t_{BR}$ otherwise:

$$\boldsymbol{I} = \begin{bmatrix} I_{1,1} & \dots & I_{1,M} \\ \vdots & \ddots & \vdots \\ I_{N,1} & \dots & I_{N,M} \end{bmatrix}.$$

The decomposition reads $\boldsymbol{I} = \mathbf{U}\boldsymbol{\Sigma}\mathbf{V}^T$, where $\mathbf{U}$ contains the spatial modes, $\boldsymbol{\Sigma}$ the singular values, and $\mathbf{V}^T$ their temporal evolution. Thus,

$$I(x_i, t_j) = \sum_{k=1}^{N_{\text{Components}}} \sigma_k U_k(x_i) V_k^T(t_j), \tag{8}$$

with $N_{\text{Components}} = 4$.

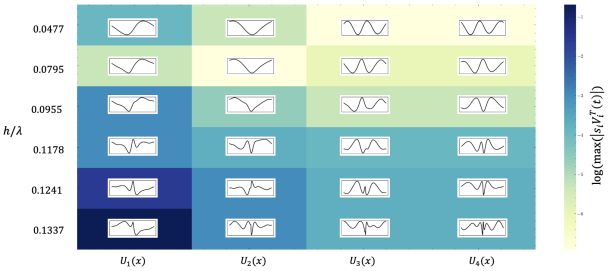


Fig. 19 Graph showing the 4 principal components of instabilities for each steepness value ordered by amplitude in log scale

Fig. 19 shows the spatial structures of the four leading SVD modes for the different steepness values. The horizontal axis represents the horizontal coordinate x, while the vertical axis represents the corresponding normalised spatial mode amplitude. All modes are nor-

malised to the same maximum absolute amplitude to facilitate comparison of their spatial structures.

At low steepness, the first mode exhibits a dominant sinusoidal structure, while the second mode is approximately phase-shifted by $\pi/2$. The third and fourth modes form another phase-shifted pair, corresponding to a second spatial pattern.

For $h/\lambda = 0.0955$, nonlinear interactions progressively deform the modal structures and introduce higher-frequency contributions. At $h/\lambda = 0.1178$, the first mode exhibits a new dominant instability while retaining some features of the mode observed at lower amplitudes. This suggests a form of interaction between the first and third modes, which were more clearly distinguishable at lower amplitudes. This interpretation is also supported by the reduction of the amplitude ratio between the third and first components to approximately 3.5. A similar observation applies to the second and fourth modes.

Near the breaking threshold, at $h/\lambda = 0.1241$, the first mode develops a clear dipolar structure. At $h/\lambda = 0.1337$, this dipolar structure remains dominant and can be interpreted as the preceding mode modified by a contribution resembling the lowest steepness first mode, but with opposite sign.

As explained above, several competing instabilities are present in Stokes waves. In our case, it is complicated to precisely characterise the instabilities and the interaction modes responsible for them. First, this complexity arises because we stabilise the wave by estimating the crest speed, which in a way biases the wave phase. Furthermore, even though the SVD effectively distinguishes the modes at low amplitudes, the constraint of orthogonality in the mathematical sense may not hold much physical significance when nonlinearities are strong. This could be another source of uncertainty when the modes have energies that are quite close to each other.

However, we managed to obtain some interesting information. We retained four modes in our analysis. Fig. 20 should be thought as a comparison with Fig. 13. The shapes of the fourth mode (third in terms of energy) derived via SVD applied to our instability signal should be compared with the shapes of the eigenmodes obtained through linear instability analysis discussed above. When nonlinearities become significant especially near the wave-breaking threshold, the modes begin to merge under the constraint of orthogonality. Fig. 20 tells us that even when considering only the mode capturing the third-highest energy level (with the maximum being captured by the dipole at the two largest values of the steepness), we can reproduce a scenario that closely approximates the theoretical description of the superharmonic instability. This suggests that it is indeed one of the mechanisms contributing effectively to wave breaking.

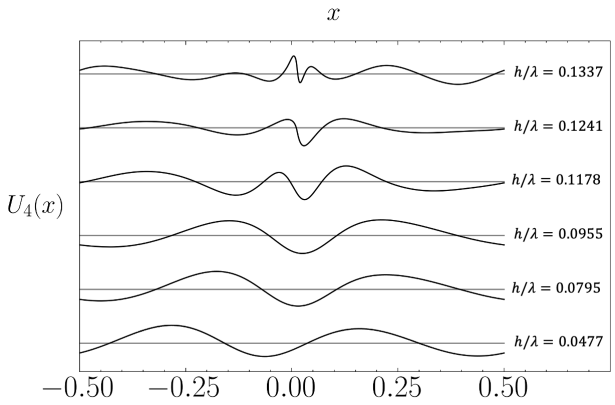


Fig. 20 Evolution of the 4th mode of the SVD as the steepness increases.

3. Conclusion

Even though we considered 3D instabilities in this review, the instabilities only applied to basic waves that are 2D. The next step is to redo the whole instability analysis (theory and numerical simulations) for waves that are genuinely 3D. The simplest 3D waves are the short-crested waves. The work is ongoing.

Acknowledgment

FD and AM acknowledge funding from the European Research Council via grant 833125-HIGHWAVE. MRT acknowledges funding from the Engineering and Physical Sciences Research Council via grants UKRI070 and UKRI3646. FD thanks the organisers of the 16th International Conference on Hydrodynamics (ICHD 2026), which took place on April 14–18, 2026, at Macau University of Science and Technology (MUST), for the invitation to give a keynote talk. This short paper is mostly based on the keynote talk.

AUTHOR DECLARATIONS

Conflict of Interest All authors declare that there are no other competing interests.

Data Availability Statements

Data sharing is not applicable to this article as no new data were created or analyzed in this study.

Ethics Approval and Consent to Participate

Not applicable.

References

[1] Hunt J. Nonlinear and wave theory contributions of T. Brooke Benjamin (1929–1995) [J]. *Annu. Rev. Fluid Mech.*, 2006, 38: 1-25.

[2] Benjamin T B, Feir J E. The disintegration of wave trains on deep water. Part I. Theory [J]. *J. Fluid Mech.*, 1967, 27: 417-430.

[3] Benjamin T B. Instability of periodic wave trains in nonlinear dispersive systems [J]. *Proceedings of the Royal Society of London. Series A, Mathematical and Physical Sciences*, 1967, 299: 59-75.

[4] Dudley J M, Genty G, Mussot A, et al. Rogue waves and analogies in optics and oceanography [J]. *Nature Reviews Physics*, 2019, 1: 675-689.

[5] Wang P, Yao Y, Tulin M P. An efficient numerical tank for non-linear water waves, based on the multi-subdomain approach with BEM [J]. *International Journal for Numerical Methods in Fluids*, 1995, 20: 1315-1336.

[6] Dauxois T. Fermi, Pasta, Ulam, and a mysterious lady [J]. *Physics Today*, 2008: 55-57.

[7] Longuet-Higgins M S. The instabilities of gravity waves of finite amplitude in deep water. I. Superharmonics [J]. *Proceedings of the Royal Society of London. Series A, Mathematical and Physical Sciences*, 1978, 360: 471-488.

[8] Longuet-Higgins M S. The instabilities of gravity waves of finite amplitude in deep water. II. Subharmonics [J]. *Proceedings of the Royal Society of London. Series A, Mathematical and Physical Sciences*, 1978, 360: 489-505.

[9] McLean J W. Instabilities of finite-amplitude water waves [J]. *Journal of Fluid Mechanics*, 1982, 114: 315-330.

[10] Babanin A. Breaking and dissipation of ocean surface waves [M]. Cambridge University Press, 2011.

[11] Jillians W J. The superharmonic instability of Stokes waves in deep water [J]. *Journal of Fluid Mechanics*, 1989, 204: 563-579.

[12] Longuet-Higgins M S, Dommermuth D G. Crest instabilities of gravity waves. Part 3. Nonlinear development and breaking [J]. *J. Fluid Mech.*, 1997, 336: 33-50.

[13] Mansar A, Turner M R, Bridges T J, et al. Effect of real-world perturbations on wave breaking due to a sharp-crested superharmonic instability [J]. *Water Waves*, 2025, 7: 159-198.

[14] Melville W K. The instability and breaking of deep-water waves [J]. *Journal of Fluid Mechanics*, 1982, 115: 165-185.

[15] Meiron D I, Saffman P G, Yuen H C. Calculation of steady three-dimensional deep-water waves [J]. *Journal of Fluid Mechanics*, 1982, 124: 109-121.

[16] Su M Y, Bergin M, Marler P, et al. Experiments on nonlinear instabilities and evolution of steep gravity-wave trains [J]. *Journal of Fluid Mechanics*, 1982, 124: 45-72.

[17] Su M Y. Three-dimensional deep-water waves. Part 1. Experimental measurement of skew and symmetric wave patterns [J]. *Journal of Fluid Mechanics*, 1982, 124: 73-108.

[18] Shrira V, Badulin S, Kharif C. A model of water wave "horse-shoe" patterns [J]. *J. Fluid Mech.*, 1996, 318: 375-405.

[19] Kharif C. Etude comparative des instabilités tridimensionnelles et bidimensionnelles des vagues de gravité de fortes cambrures [J]. *J. Mech. Th. Appl.*, 1987, 6: 843-864.

[20] Kharif C, Ramamonjiarisoa A. Deep water gravity wave instabilities at large steepness [J]. *Phys. Fluids*, 1988, 31: 1286-1288.

[21] Kharif C, Ramamonjiarisoa A. On the stability of gravity waves on deep water [J]. *J. Fluid Mech.*, 1990, 218: 163-170.

[22] Tanaka M. The stability of steep gravity waves. Part 2 [J]. *Journal of Fluid Mechanics*, 1985, 156: 281-289.

[23] Banner M L, Peregrine D H. Wave breaking in deep water [J]. *Annu. Rev. Fluid Mech.*, 1993, 25: 373-397.

[24] Popinet S. Gerris: a tree-based adaptive solver for the incompressible Euler equations in complex geometries [J]. *Journal of Computational Physics*, 2003, 190(2): 572-600.

[25] Popinet S. An accurate adaptive solver for surface-tension-driven interfacial flows [J]. *Journal of Computational Physics*, 2009, 228(16): 5838-5866.

[26] Basilisk [EB/OL]. http://basilisk.fr/.

[27] Chen G, Kharif C, Li J. Two-dimensional Navier-Stokes simulation of breaking waves [J]. *Physics of Fluids*, 1997, 11: 121-133.

[28] Iafrati A. Numerical study of the effects of the breaking intensity on wave breaking flows [J]. *Journal of Fluid Mechanics*, 2009, 622: 371-411.

[29] Iafrati A. Energy dissipation mechanisms in wave breaking processes: Spilling and highly aerated plunging breaking events [J]. *Journal of Geophysical Research: Oceans*, 2011, 116(C7).

[30] Deike L, Popinet S, Melville K. Capillary effects on wave breaking [J]. *J. Fluid Mech.*, 2015, 769: 541-569.

[31] Deike L, Melville K, Popinet S. Air entrainment and bubble statistics in breaking waves [J]. *Journal of Fluid Mechanics*, 2016, 801: 91-129.

[32] Mostert W, Popinet S, Deike L. High-resolution direct simulation of deep water breaking waves: Transition to turbulence, bubbles and droplets production [J]. *Journal of Fluid Mechanics*, 2022, 942: A27.

[33] Fenton J D. A fifth-order Stokes theory for steady waves [J]. *Journal of Waterway, Port, Coastal, and Ocean Engineering*, 1985, 111(2): 216-234.

[34] Jolliffe I T. Principal component analysis [M]. 2nd ed. Springer, 2002.